Model-Free Fuzzy Adaptive Control of the Heading Angle of Fixed-Wing Unmanned Aerial Vehicles

Shulong Zhao[1]; Xiangke Wang[2]; Daibing Zhang[3]; and Lincheng Shen[4]

Abstract: In this paper, a novel model-free fuzzy adaptive control (MFFAC) scheme is developed to control the heading angle of fixed-wing unmanned aerial vehicles (UAVs). It is common knowledge that the aerodynamics of the heading angle of fixed-wing UAVs are difficult to accurately model and are subject to wind disturbances. Therefore, it is difficult to implement conventional model-based control to the heading angle control problem. To overcome this difficulty, the authors propose a novel data-driven control approach. First, an adaptive neuro-fuzzy inference system (ANFIS) is designed to estimate the pseudo partial derivative (PPD), which is described as an equivalent dynamic linearization (EDL) technique for unknown nonlinear systems. Secondly, an extended model-free adaptive control (MFAC) strategy is proposed to control the heading angle of fixed-wing UAVs with wind disturbances. Finally, a discrete Lyapunov-based stability analysis is presented to prove the globally asymptotic stability of the proposed control scheme. The high-fidelity semiphysical simulations illustrate that accurate and stable control is achieved in this designed control strategy. **DOI: 10.1061/(ASCE)AS.1943-5525.0000730.**

Introduction

Unmanned aerial vehicles (UAVs) have been widely used in both civilian and military missions. A variety of control algorithms have been developed to ensure that the UAV moves smoothly and steadily (Warsi et al. 2014; Chao et al. 2007, 2010; Wang et al. 2016a). Fixed-wing vehicles, each equipped with a propeller and a set of control surfaces (elevator, ailerons, and rudder), have been employed in a variety of cases (Sujit et al. 2014). Many tasks or applications, such as path following and obstacle avoidance, require that the vehicles are able to handle complex and changing environments and follow the predefined trajectory efficiently and accurately (Brezoescu et al. 2013; Paw and Balas 2011; Wang et al. 2016b).

The motion principle and control methods of fixed-wing UAVs are different from those of quadrotors or helicopters (Ren and Beard 2004). When a fixed-wing vehicle makes a turn, all the control surfaces must be involved. An elevator is employed to maintain a proper altitude against the gyroscopic effect. The fuselage is diverted by ailerons in order to offer centripetal acceleration of circular motion. Meanwhile, the rudder adjusts the heading angle of the vehicle along the direction of airspeed (Cabecinhas et al. 2007).

The most popular methods for controlling the heading angle of fixed-wing UAVs involve adopting proportional-integral-derivative (PID) frameworks (Mystkowski 2013). However, in those methods, the selection and tuning of the parameters of the controller, which are prone to pollution by disturbances and noises, present the greatest challenges. An automatic parameter-tuning method was proposed (Poksawat et al. 2016) for attitude control of fixed-wing UAVs. In this study, the mathematical model of the UAV was obtained via frequency identification, but it is difficult to utilize directly in flight tests. To address this problem, Cai et al. (2008) used a composite nonlinear feedback technique to model and control the yaw channel of the UAV. However, uncertainties and disturbances are rarely considered in the previously mentioned methods. The heading angle of the UAV was controlled via a saturation feedback scheme by Ren and Beard (2004), who addressed uncertainties and disturbances under the input-to-state (ISS) framework. Guo and Liu (2012) proposed an adaptive dynamic surface control for the flight path angle using a neural network to estimate uncertainties and disturbances.

However, it was assumed in many studies that there exists a coordinated turn or level flight condition (Beard et al. 2002, 2014; Sujit et al. 2014; Mahony et al. 2016; Ren and Beard 2004; Guo and Liu 2012), which is a sought-after flight condition in manned flight for reasons of passenger comfort by guaranteeing that the vehicle turns without skidding laterally (Nabaa and Bishop 2000). Unfortunately, this condition is vague and difficult to implement, because most uncertainties and disturbances of the heading angle are present in the sliding effects for fixed-wing UAVs. Although the rudder is designed to have an inherent role in reducing the sideslip angle for most fixed-wing UAVs (Luo et al. 2011), it is difficult to ensure that the sideslip angle is maintained at zero. In addition, the kinematic equation of the heading angle is hard to depict precisely, and it is costly and time consuming to obtain the kinematic equations for small UAVs via wind tunnel tests or system identification (Beard et al. 2014).

Hou et al. proposed a model-free adaptive control (MFAC) strategy to design the controller such that only the set of input-output (I/O) data is required (Hou and Jin 2011a, b; Hou and Bu 2011), and this approach has been developed for a class of nonaffine

[1]Ph.D. Candidate, College of Mechanics and Automation, National Univ. of Defense Technology, Changsha 410075, People's Republic of China (corresponding author). ORCID: http://orcid.org/0000-0002-9610-962X. E-mail: jaymaths@nudt.edu.cn

[2]Professor, College of Mechanics and Automation, National Univ. of Defense Technology, Changsha 410075, People's Republic of China. E-mail: xkwang@nudt.edu.cn

[3]Professor, College of Mechanics and Automation, National Univ. of Defense Technology, Changsha 410075, People's Republic of China. E-mail: swimsword@163.com

[4]Professor, College of Mechanics and Automation, National Univ. of Defense Technology, Changsha 410075, People's Republic of China. E-mail: lcshen@nudt.edu.cn

Note. This manuscript was submitted on January 12, 2016; approved on December 12, 2016; published online on February 23, 2017. Discussion period open until July 23, 2017; separate discussions must be submitted for individual papers. This paper is part of the ***Journal of Aerospace Engineering***, © ASCE, ISSN 0893-1321.

discrete nonlinear systems. Based on the equivalent dynamic linearization (EDL) technique, a time-varying parameter, i.e., the pseudo partial derivative (PPD), is employed to estimate the dynamic characters of the closed-loop system. The control scheme is implemented via the gradient descent of the cost function in recursive form. Compared with other data-driven control algorithms, the MFAC is simple and easy to implement (Hou and Wang 2013).

Motivated by the idea of a modified strategy called model-free fuzzy adaptive control (MFFAC), the authors propose a MFFAC for the heading angle of fixed-wing UAVs in this paper. The main advantage is that it is robust to disturbance and the sideslip will be eliminated actively, and the PPD is estimated via an adaptive neuro-fuzzy inference system (ANFIS), which performs better than the feedforward neural networks. Consequently, the proposed controller is easy to implement. There is no need for the costly and extremely time-consuming process of system identification. The proposed framework has the following contributions:

1. A MFFAC control scheme for the heading angle of a fixed-wing UAV is proposed, and the discrete Lyapunov technology is employed to prove the stability of the proposed controller and the convergence of the tracking error.
2. The PPD is estimated by the ANFIS learning via the back-propagation error concept and the gradient descent algorithm. It could be obtained by a fuzzy system possessing the capability of learning and self-adaptive adjustment.
3. High-fidelity semiphysical simulations are performed to illustrate the applicability of the developed control strategy.

To the authors' best knowledge, although the heading control methods for fixed-wing UAVs have been reported in many applications (Warsi et al. 2014; Beard et al. 2014; Ren and Beard 2004; Luo et al. 2011; Cabecinhas et al. 2007; Mystkowski 2013; Poksawat et al. 2016; Cai et al. 2008; Guo and Liu 2012), this is the first time the MFFAC has been applied to fixed-wing UAVs.

Preliminaries and Formulation

Preliminaries on MFFAC

Considering a class of discrete single input single output (SISO) system

$$y(k+1) = f[y(k), \ldots, y(k-n_y), u(k), \ldots, u(k-n_u)] \quad (1)$$

where $y(k) \in \mathbf{R}$, $u(k) \in \mathbf{R}$ = output and input of the system at time index k, respectively; n_y and n_u = unknown positive constants; and $f(\cdot)$ = unknown nonlinear function.

Assumption 1 (Hou and Jin 2011b): The partial derivative of $f(\cdot)$ with respect to $u(k)$ is continuous.

Assumption 2 (Hou and Jin 2011b): The system (1) is generalized Lipschitz. That is

$$|\Delta y(k+1)| \le L|\Delta u(k)| \quad (2)$$

where $L > 0$ is a constant, $\Delta y(k+1) = y(k+1) - y(k)$, and $\Delta u(k) = u(k) - u(k-1)$.

Remark 1: Assumption 1 is a typical condition for a general nonlinear system, and Assumption 2 is a limitation on the rate of changes of the controlled plant. Many practical plants can satisfy this constraint, such as the temperature system and pressure system.

Under these assumptions, there must exist a time-varying parameter $\phi(k)$, called the PPD, satisfying the following data model (see Hou and Jin 2011a, b for details):

$$\Delta y(k+1) = \phi(k)\Delta u(k), \quad \text{for } \Delta u(k) \neq 0 \quad (3)$$

where $|\phi(k)| \le L$ is satisfied for all time.

System (3) is an equivalent dynamic linearization presentation to the original controlled system (1).

According to Hou and Jin (2011a), the MFFAC controller is given as

$$u(k) = u(k-1) + \frac{\rho\phi(k)}{\lambda + |\phi(k)|^2}[y^*(k+1) - y(k)] \quad (4)$$

where λ = punishment factor; $\rho \in (0, 1]$ = step factor; and $y^*(k+1)$ = desired output.

PPD $\phi(k)$ is, obviously, a time-varying parameter even though the controlled system is a time-invariant system. A formula was also proposed by Hou and Jin (2011a) to estimate the PPD

$$\hat{\phi}(k) = \hat{\phi}(k-1) + \frac{\eta\Delta u(k-1)}{\mu + |\Delta u(k-1)|^2}[\Delta y(k) - \hat{\phi}(k-1)\Delta u(k-1)] \quad (5)$$

where $\mu > 0$ = punishment factor and $\eta \in (0, 1]$ = step factor.

Dynamics of the Heading Angle for a Fixed-Wing UAV

The motion properties of the heading angle of a fixed-wing UAV can be treated as the motion of a rigid body, which can be expressed as

$$\dot{\psi} = \omega \quad (6)$$

$$J\dot{\omega} + c\omega + d = \tau(a, r)$$

where ψ = yaw; ω = angle rate of ψ; J = moment of inertial; c = related Coriolis force; d = disturbance, where $|d| < d_m$ and d_m is an unknown positive constant; $\tau(a, r) = [\tau(a), \tau(r)]$ = control inputs; and a and r = effects of the aileron and the rudder, respectively.

Defining $y = \omega$ and $\tau(a, r) = u_{a,r} = [u_a, u_r]$, then one can obtain

$$J\dot{y} + cy + d = u_{a,r} \quad (7)$$

Using the first order Euler's method, the discretization form of (7) is as follows:

$$\frac{y(k+1) - y(k)}{\Delta T} = -\frac{c(k)}{J(k)}y(k) - \frac{d(k)}{J(k)} + \frac{u_{a,r}(k)}{J(k)} \quad (8)$$

where ΔT = sampling time.

The simplified form of (8) is given as

$$y(k+1) = M(k)y(k) - D(k) + N(k)u_{a,r}(k) \quad (9)$$

where $M(k) = \{[J(k) - c(k)\Delta T]/J(k)\}$; $D(k) = \{[d(k)\Delta T]/J(k)\}$; and $N(k) = [\Delta T/J(k)]$.

Employing the equivalent dynamic linearization (EDL) technology defined by Hou and Bu (2011), one can obtain

$$\Delta y(k+1) = \Phi(k)[\Delta y(k), \Delta u_{a,r}(k)]^T \quad (10)$$

where $\Phi(k) = [\phi_y(k), \phi_{ua}(k), \phi_{ur}(k)]$ is the PPD and $\Delta y(k) = y(k) - y(k-1)$, $\Delta u_{a,r}(k) = u_{a,r}(k) - u_{a,r}(k-1)$. The control inputs can be written as $\Delta u_{a,r}(k) = [\Delta u_a(k), \Delta u_r(k)]$. $u_a = \tau(a)$, $u_r = \tau(r)$ represent the surface angles of the aileron and the rudder, respectively.

Remark 2: The PPD in (10) has the form

$$\Phi(k) = H_{y,u}(k-1) + \left[\frac{\partial y(k+1)}{\partial y(k)}, \frac{\partial y(k+1)}{\partial u_{a,r}(k)}\right] \quad (11)$$

where $H_{y,u}(k-1)$ is a solution of $\Omega(k) = H_{y,u}(k-1)[\Delta y(k), \Delta u_{a,r}(k)]^T$, and $\Omega(k) = M(k)y(k-1) + D(k-1) + N(k)u_{a,r}(k-1) - M(k-1)y(k-1) - D(k) + N(k-1)u_{a,r}(k-1)$ is employed in the

EDL technology. For $\Delta y(k) \neq 0$ and $\Delta u_{a,r}(k) \neq 0$, a unique solution of $H_{y,u}(k-1)$ can certainly be found.

MFFAC Control Strategy

Estimation of the PPD

The authors estimate the PPD using the ANFIS technology. The ANFIS is a hybrid technique that combines the properties of both neural networks and the Takagi-Sugeno (T-S) fuzzy system. To be more specific, during the learning procedures of neural networks, the fuzzy system possesses the capability of learning and self-adaptive adjustment (see Jang and Sun 1995 for details). The ANFIS analyzed here has a five-layer architecture (Fig. 1) with four inputs and three outputs as illustrated in the following.

Inputs

1. Difference in the heading angle in time index $k+1$ and k, i.e., $\Delta y(k+1)$, $\Delta y(k)$; and
2. Difference in the aileron and rudder surface angle in time index k, i.e., $\Delta u_a(k) = u_a(k) - u_a(k-1)$, $\Delta u_r(k) = u_r(k) - u_r(k-1)$.

Outputs

1. First element of the PPD, $\phi_y(k)$;
2. Second element of the PPD, $\phi_{ua}(k)$; and
3. Third element of the PPD, $\phi_{ur}(k)$.

A fuzzy neural network can be used to approximate any continuous function to an arbitrary accuracy. Every segment of the neural network could be fuzzified in theory, and the input data are fuzzified here. The if-then rule is

If $X(k)$ is in F_i, then $f_i = PX(k) + R$

where $X = [\Delta y(k+1), \Delta y(k), \Delta u_a(k), \Delta u_r(k)]$ = input vector; f_i = output of the rule; and F_i = ith fuzzy set with regard to X. $P \in \mathbf{R}^{3\times 4}$ and $R \in \mathbf{R}^3$ are the consequent parameters.

The five layers are illustrated as follows:

Layer 1: Each node in this layer is an adjustable node. The input vector is X, and the output $O_{1,i} = \mu_{F_i}(X)$ is the membership function, which usually adopts a Gaussian function

$$O_{1,i} = \mu_{F_i}(X) = \exp\left[-\frac{(X-X_i)^T(X-X_i)}{2b_i^2}\right], \quad i = 1,2 \tag{12}$$

where X_i and b_i = constants that represent the centers and the widths of the Gaussian functions, respectively.

Layer 2: Each node in this layer is a fixed node. The outputs of this layer can be represented as

$$O_{2,i} = \omega_i = \mu_{F_1}(X)\mu_{F_2}(X) \tag{13}$$

Layer 3: Each node in this layer is a fixed node that plays a normalization role in the former layer. The outputs of this layer can be represented as

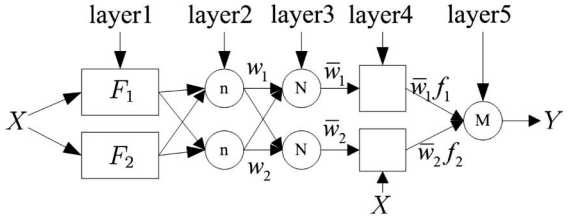

Fig. 1. Adaptive neuro-fuzzy inference system structure

$$O_{3,i} = \bar{\omega}_i = \frac{\omega_i}{\sum_{i=1}^{2}\omega_i} \tag{14}$$

Layer 4: The nodes are adaptive nodes. The output of each node is a first-order polynomial

$$O_{4,i} = \bar{\omega}_i f_i = \bar{\omega}_i[PX(k) + R], \quad i = 1,2 \tag{15}$$

Layer 5: There is only one fixed output node in this layer, and it is given by

$$O_{5,i} = Y(k) = \frac{\sum_{i=1}^{2}\omega_i f_i}{\sum_{i=1}^{2}\omega_i} \tag{16}$$

where $Y = [\phi_y(k), \phi_{ua}(k), \phi_{ur}(k)]$ = output vector. To simplify this analysis, the output vector can be written as

$$Y(k) = \Theta(k)\xi(k)$$

where $\Theta(k)$ and $\xi(k)$ are regarded as parameters of the adaptive networks.

The ANFIS is trained with data obtained from the controlled system. Parameters X_i and b_i in the membership functions and the consequent parameters P and R are learned by the back-propagation error concept and the gradient descent algorithm. The output error for each time index is defined as

$$E(k) = [\Phi(k) - \hat{\Phi}(k)][\Phi(k) - \hat{\Phi}(k)]^T \tag{17}$$

where $\hat{\Phi}(k)$ = estimation of the PPD. The weights are adaptively adjusted using the gradient descent algorithm

$$W(k+1) = W(k) - \kappa(k)\frac{\partial E}{\partial W} \tag{18}$$

where $W(k) = W(X_i, b_i, P, R)$ represents the parameters and $\kappa(k)$ = learning rate. To confirm that the PPD is bounded, the authors give the following two lemmas. Specifically, Lemma 1 guarantees the boundedness of the estimated error, while Lemma 2 shows that the estimated PPD is bounded. As a result, the boundedness of the PPD can be readily derived.

Lemma 1 (Jang and Sun 1995; Wang and Er 2016): A time-varying parameter $\Phi(k)$ is given as

$$\Phi(k) = g(\Delta y, \Delta u_a, \Delta u_r) \tag{19}$$

where $g(\cdot)$ = continuous function. For any $\epsilon > 0$, there exists a proper weight vector Θ^* and $\xi(k)$ such that the ANFIS can approximate the $\Phi(k)$ within the error bound ϵ by suitably selecting the parameters X_i and b_i

$$g(\Delta y, \Delta u_a, \Delta u_r) = \hat{\Phi}(k) + \epsilon_m = \Theta^*\xi(k) + \epsilon_m \tag{20}$$

where ϵ_m = error with $|\epsilon_m| < \epsilon$.

The estimation cost function is defined as

$$J_\Phi(k) = \frac{\zeta}{2}[\Delta y - \hat{\Phi}(k)\Delta u(k)]^2 + \frac{\pi}{2}[\hat{\Phi}(k) - \hat{\Phi}(k-1)]^2 \tag{21}$$

where ζ and π = weight constants. The adaptive law of the parameter θ is

$$\theta(k+1) = \theta(k) - \gamma(k)\frac{\partial J_\Phi(k)}{\partial\theta(k)} \tag{22}$$

Lemma 2: Given the cost function (21) and adaptive law (22), the PPD $\hat{\Phi}(k)$ is bounded if the learning rate $\gamma(k)$ and weight parameters π satisfy

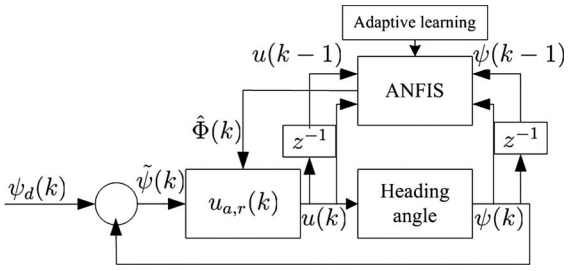

Fig. 2. Control scheme

$$0 < \gamma(k) < \frac{2}{\pi + \Delta u^2(k-1)}$$
$$\pi < \zeta |\Delta u_M^2| \tag{23}$$

where $|\Delta u_M| = \sup |\Delta u(k)|$.

Control Scheme

Assumption 3: There is little prior knowledge about the desired output $y_d(k)$ and it is assumed that

$$0 < \Delta y_d(k+1) < \epsilon, \quad \text{then } [\Delta y_d(k+1)]^2 \approx 0 \tag{24}$$

where $\Delta y_d(k+1) = y_d(k+1) - y_d(k)$; and ϵ = sufficient small constant.

The control scheme can be expressed as in Fig. 2.

Theorem 1: Define the heading angle error $\tilde{\psi}(k) = \psi_d(k) - \psi(k)$, the angle rate error $\tilde{\omega}(k) = \omega_d(k+1) - \omega(k)$, and the estimation error of the PPD $\tilde{\Phi}(k) = \hat{\Phi}(k) - \Phi(k)$, where the PPD of the system is estimated by the ANFIS. Parameters $0 < k_1 < 2$, $\lambda(k) > 0$, $0 < \eta(k) < (\Phi_M / \check{\Phi}_M)$, Φ_M and $\check{\Phi}_M$ are defined in the proof. The controller of nonlinear system (6) is designed as

$$u(a,r)(k) = u(a,r)(k-1) + \frac{\eta(k)\hat{\Phi}(k)}{\lambda(k) + \|\hat{\Phi}(k)\|^2}[k_1\tilde{\psi}(k) + \tilde{\omega}(k)] \tag{25}$$

which guarantees that $\lim_{k\to\infty}[\psi_d(k) - \psi(k)] = 0$.

Proof: According to the definition of a heading angle error, one can obtain

$$\begin{aligned}\tilde{\psi}(k+1) &= \psi_d(k+1) - \psi(k+1)\\ &= \psi_d(k+1) - \psi(k) - \Delta T\omega(k)\\ &= \psi_d(k+1) - \psi_d(k) + \psi_d(k) - \psi(k) - \Delta T\omega(k)\\ &= \Delta\psi_d(k+1) + \tilde{\psi}(k) - \Delta T\omega(k)\end{aligned} \tag{26}$$

where $\Delta\psi_d(k+1) = \psi_d(k+1) - \psi_d(k)$ and $\Delta u(k) = [\Delta y, \Delta u_a, \Delta u_r]$ is the differential of the control input.

The system (6) can be divided into two subsystems:

1. $\tilde{\psi}(k)$ subsystem

The discrete Lyapunov function is defined as

$$V_1(k) = \frac{1}{2}\tilde{\psi}^2(k) \tag{27}$$

Thus, the change of the Lyapunov function can be given by

$$\begin{aligned}\Delta V_1(k) &= V_1(k+1) - V_1(k) = \frac{1}{2}\tilde{\psi}^2(k+1) - \frac{1}{2}\tilde{\psi}^2(k)\\ &= \frac{1}{2}[\Delta\psi_d(k+1) + \tilde{\psi}(k) - \Delta T\omega(k)]^2 - \frac{1}{2}\tilde{\psi}^2(k)\end{aligned} \tag{28}$$

If $\omega(k)$ is chosen as $\omega^*(k) = \frac{1}{\Delta T}\Delta\psi_d(k+1) + k_1\tilde{\psi}(k)$, then

$$\Delta V_1(k) = \frac{1}{2}[(1-k_1)^2 - 1]\tilde{\psi}^2(k) \tag{29}$$

Because $0 < k_1 < 2$, it follows that $\Delta V_1(k) \le 0$ and $\Delta V_1(k) = 0$ when $\tilde{\psi}(k) = 0$.

2. $\tilde{\omega}(k)$ subsystem

If $\tilde{\omega}(k) = \omega^*(k) - \omega(k)$, then one can obtain

$$\begin{aligned}\tilde{\omega}(k+1) &= \omega^*(k+1) - \omega(k+1)\\ &= \omega^*(k+1) - \omega(k) - \Phi(k)\Delta u(k)\\ &= \omega^*(k+1) - \omega^*(k) + \omega^*(k) - \omega(k) - \Phi(k)\Delta u(k)\\ &= \Delta\omega^*(k) + \tilde{\omega}(k) - \Phi(k)\Delta u(k)\end{aligned} \tag{30}$$

where $\Delta\omega^*(k) = \omega^*(k+1) - \omega^*(k)$.

From (30), it is clear that

$$\begin{aligned}\Delta u(a,r)(k) &= \frac{\eta(k)\hat{\Phi}(k)}{\lambda(k) + |\Phi(k)|^2}[k_1\tilde{\psi}(k) + \tilde{\omega}(k)]\\ &= \frac{\eta(k)\hat{\Phi}(k)}{\lambda(k) + |\Phi(k)|^2}[k_1\tilde{\psi}(k) + \omega_d(k+1) - \cdots - \omega^*(k+1)\\ &\quad + \omega^*(k+1) - \omega^*(k) + \omega^*(k) - \omega(k)]\end{aligned} \tag{31}$$

Obviously, $\omega_d(k+1) = \{[\psi_d(k+1) - \psi_d(k)]/\Delta T\}$. Then,

$$\Delta u(a,r)(k) = \frac{\eta(k)\hat{\Phi}(k)}{\lambda(k) + |\Phi(k)|^2}[\Delta\omega^*(k) + \tilde{\omega}(k)] \tag{32}$$

Then, $\tilde{\omega}(k+1)$ can be rewritten as

$$\tilde{\omega}(k+1) = [\Delta\omega^*(k+1) + \tilde{\omega}(k)](1 - \Gamma) \tag{33}$$

where $\Gamma = \{[\eta(k)\hat{\Phi}(k)\Phi(k)]/[\lambda(k) + |\Phi(k)|^2]\}$.

One considers

$$\tilde{\Phi}(k+1) = \hat{\Phi}(k+1) - \Phi(k+1) \tag{34}$$

With Lemma 1 and $\Theta^*(k+1) = \Theta^*(k) = \Theta$, one can obtain

$$\begin{aligned}\tilde{\Phi}(k+1) &= \Theta(k+1)\xi(x) - \Theta(k+1)\xi(x) - \epsilon_m\\ &= [\Theta(k+1) - \Theta^*(k)]\xi(x) - \epsilon_m\\ &= [\Lambda_1\Theta(k) - \Lambda_2 - \Theta^*(k)]\xi(x) - \epsilon_m\end{aligned} \tag{35}$$

where $\Lambda_1 = 1 - \gamma(k)[\pi + \Delta u^2(k-1)]\xi^2(k)$ and $\Lambda_2 = [\pi\hat{\Phi}(k-1) - \zeta\Delta y(k)\Delta u(k-1)]\xi(k)$. The definitions of Λ_1 and Λ_2 can be found in the Appendix.

The discrete Lyapunov function can be defined as

$$V_2(k) = \frac{1}{2}\tilde{\psi}^2(k) + \frac{1}{2}\tilde{\omega}^2(k) + \frac{1}{2}\tilde{\Phi}^2(k) \tag{36}$$

The change in the Lyapunov function can be given by

$$\begin{aligned}\Delta V_2(k) &= V_2(k+1) - V_2(k)\\ &= \frac{1}{2}\tilde{\psi}^2(k+1) - \frac{1}{2}\tilde{\psi}^2(k) + \frac{1}{2}\tilde{\omega}^2(k+1) - \cdots - \frac{1}{2}\tilde{\omega}^2(k) + \frac{1}{2}\tilde{\Phi}^2(k+1) - \frac{1}{2}\tilde{\Phi}^2(k) = \frac{1}{2}[(1-k_1)^2 - 1]\tilde{\psi}^2(k)\\ &\quad + \frac{1}{2}[\Delta\omega^*(k+1) + \tilde{\omega}(k)]^2(1-\Gamma)^2 - \cdots - \frac{1}{2}\tilde{\omega}^2(k) + \frac{1}{2}\{[\Lambda_1\Theta(k) - \Lambda_2 - \Theta^*(k)]\xi(x) - \epsilon_m\}^2 - \cdots - \frac{1}{2}\{[\Theta(k) - \Theta^*(k)]\xi(x) - \epsilon_m\}^2\\ &\le \frac{1}{2}[(1-k_1)^2 - 1]\tilde{\psi}^2(k) + \frac{1}{2}\{[\Gamma^2 - 1]\tilde{\omega}^2(k) + \cdots + 2\tilde{\omega}(k)\Delta\omega^*(k+1)\Gamma^2 + [\Delta\omega^*(k+1)\Gamma]^2\} + \cdots + \frac{1}{2}\{[\Lambda_1\Theta(k) - \Theta^*(k)]\xi(x) - \epsilon_m\}^2\\ &\quad - \frac{1}{2}\{[\Theta(k) - \Theta^*(k)]\xi(x) - \epsilon_m\}^2\\ &= \frac{1}{2}[(1-k_1)^2 - 1]\tilde{\psi}^2(k) + \frac{\Gamma^2 - 1}{2}\left\{\left[\tilde{\omega}(k) + \frac{\Gamma^2}{\Gamma^2 - 1}\right]^2 - \cdots - \frac{\Gamma^2}{(\Gamma^2 - 1)^2}[\Delta\omega^*(k+1)]^2\right\} + \cdots + \frac{1}{2}\{[\Lambda_1\Theta(k) - \Theta^*(k)]\xi(x) - \epsilon_m\}^2\\ &\quad - \frac{1}{2}\{[\Theta(k) - \Theta^*(k)]\xi(x) - \epsilon_m\}^2 \end{aligned} \tag{37}$$

Because the profile of $\psi_d(k)$ is continuous and smooth, it is reasonable to assume that $\Delta\omega^*(k+1)$ satisfies Assumption 3. Meanwhile, it is obvious that $|\Lambda_1| < 1$, so $|\Lambda_1\Theta(k)| < |\Theta(k)|$. (37) can be rewritten as

$$\Delta V_2(k) \le \frac{1}{2}[(1-k_1)^2 - 1]\tilde{\psi}^2(k) + \frac{\Gamma^2 - 1}{2}\left\{\left[\tilde{\omega}(k) + \frac{\Gamma^2}{\Gamma^2 - 1}\Delta\omega^*(k+1)\right]^2\right\} \tag{38}$$

From Lemma 2, it is obvious that $\hat{\Phi}(k)$ is bound. Also, Lemma 1 indicates that $\Phi(k)$ is also bound. For more complicity,

$$\sup|\hat{\Phi}(k)| = \hat{\Phi}_M, \qquad \sup|\Phi(k)| = \Phi_M \tag{39}$$

Define $\breve{\Phi} = \max\{\hat{\Phi}_M, \Phi_M\}$, and with parameters $\lambda(k) > 0$ and $0 < \eta(k) < (\Phi_M/\breve{\Phi}_M)$, one can obtain

$$|\Gamma| < \left|\frac{\eta(k)\breve{\Phi}^2}{\lambda(k) + |\Phi(k)|^2}\right| < \frac{|\eta(k)\breve{\Phi}^2|}{|\Phi(k)|^2} < 1 \tag{40}$$

such that $\Gamma^2 - 1 < 0$. That is to say, $\Delta V_2(k) \le 0$. When $\tilde{\psi}(k) = 0$ and $\tilde{\omega}(k) = -(\Gamma^2)/(\Gamma^2 - 1)[\Delta\omega^*(k+1)]$, then $\Delta V_2(k) = 0$.

From Lemma 1, it is obvious that $\lim_{k\to\infty}[\psi_d(k) - \psi(k)] = 0$.

Remark 3: Consider the closed loop of the heading angle, taking full advantage of the data driven control (DDC) strategy. The accurate dynamic model is dispensable, and a proper controller is designed with I/O data. The greatest advantages of the proposed method lie in its robustness to disturbance and its active elimination of sideslip rather than inherent reduction by the rudder. Meanwhile, the control algorithm (25) has no relationship with any prior knowledge of the controlled system.

Simulation and Discussion

To check the performance of the controller described in the previous sections, a high-fidelity semiphysical simulation scheme is developed. The proposed approach is simulated in an X-plane platform, which provides very accurate aircraft models and has the possibility to exchange data with external systems. The aircraft models simulated in the X-plane are built based on the exact physical model and materials. Here, the exact physical model expression of the fixed-wing UAV is not employed in the algorithm, but the I/O data are collected.

Simulation Platform

The whole system consists of three building blocks: ground station, autopilot, and X-plane, as shown in Fig. 3. The ground station is developed and employed to communicate with the X-plane by the user datagram protocol (UDP) communication. The autopilot and X-plane are connected with a network cable, which simulates a wireless transceiver. The X-plane provides tall of the movement states to the autopilot and receives control commands at the same time. The ground station is employed to record and present the

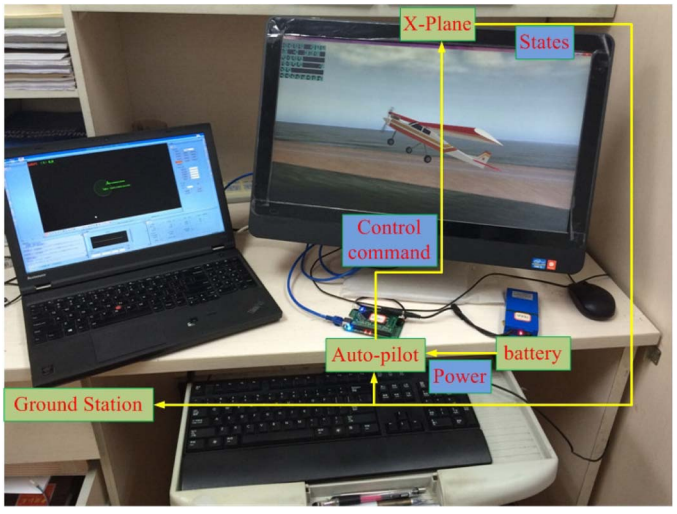

Fig. 3. High-fidelity semiphysical simulation environment, constructed by an actual autopilot, a ground station, and an X-plane flight simulator (image by Shulong Zhao)

Fig. 4. Great Planes PT-60 RC plane and its main parameters in the X-plane flight simulator

Table 1. Control Parameters

Parameter	Case 1	Case 2
ζ	2	2
π	1	1
γ	0.1	0.2
η	0.6	0.6
λ	0.25	0.22
k_1	1.5	1
Δu_m (rad)	0.7	0.7
K_p (yaw to roll)	0.8	1.2
K_i (yaw to roll)	0.5	0.5
K_d (yaw to roll)	0.01	0.01
K_p (yaw to rudder)	0.1	0.1
K_i (yaw to rudder)	0.05	0.05
K_d (yaw to rudder)	0.01	0.01

flight procedure. Some control modes and commands, such as velocity, altitude, and other path information, are sent to the autopilot directly. The autopilot, developed by the authors' work group, uses the position, orientation, heading angle, and other information of the UAV to calculate the low-level control signals.

The Great Planes PT-60 RC plane was used in the simulations. The frame of the plane with its main parameters is shown in Fig. 4.

Simulation Results

The proposed method is compared with the cascaded PID controller in an autopilot, which consists of two loops: the yaw-to-roll loop and the yaw-to-rudder loop. The inputs are the aileron and the rudder, and the output is the measured yaw angle. The major character is robust to disturbances, and two wind conditions are introduced: gust wind and turbulent wind.

One of the things that must be considered is the desired profile of the heading angle. There are two different cases of the heading angle: a fixed value of the angle rate and a changeable value of the angle rate. This is performed to achieve a better recognition of the capabilities of the actual control surfaces in the adjustment of the heading angle. The control parameters are shown in Table 1.

The results obtained for Case 1, with a fixed value of the angle rate (0.1 rad/s) and a turbulent wind (5 knots), are presented in Fig. 5. The initial and final values of the yaw are 4.54 and 5.15 rad, respectively. Because the yaw is defined within $[0, 2\pi]$, the angle returns to 0 if it exceeds 2π. The altitude of the vehicle is approximately 100 m, and the cruise velocity is 15 m/s.

The red dotted line indicates the desired angle profile, the green line indicates the angle profile of the proposed method, and the blue dashed-dotted line indicates the result of the PID controller in the figure. The tracking error of the proposed method is far less than those of the PID controller because of the active adjustment of the sideslip. Meanwhile, the mean fluctuation of the angle profile of the proposed method always lies within [−0.05 rad, 0.05 rad], which indicates a good performance in the presence of a turbulent wind.

The control inputs of the aileron and the rudder are shown in Figs. 6 and 7. During the tracking process, it is clear that the movement of the aileron is more acute than that of the rudder, but their relationship is difficult to grasp or to express via a known function. By using the I/O data cleverly, a proper and feasible controller is designed, and the predefined profile of the heading angle is well tracked.

The next simulation illuminates the controller performance in the face of gust wind and a changeable value of the angle rate. The authors use a designed curved path to obtain the profile of the heading angle, which consists of three segments: a smooth curve, an arc, and another smooth curve. The gust wind is 10 knots from 135 degrees southwest. The heading angle of the UAV in Case 2, with gust wind and a changeable value of the angle rate, is shown in Fig. 8.

The performance of the two control strategies is neck and neck without the influence of wind. When the airplane passes through the predefined path, the gust wind is added, and the performances of the proposed method and the PID are close but show a great

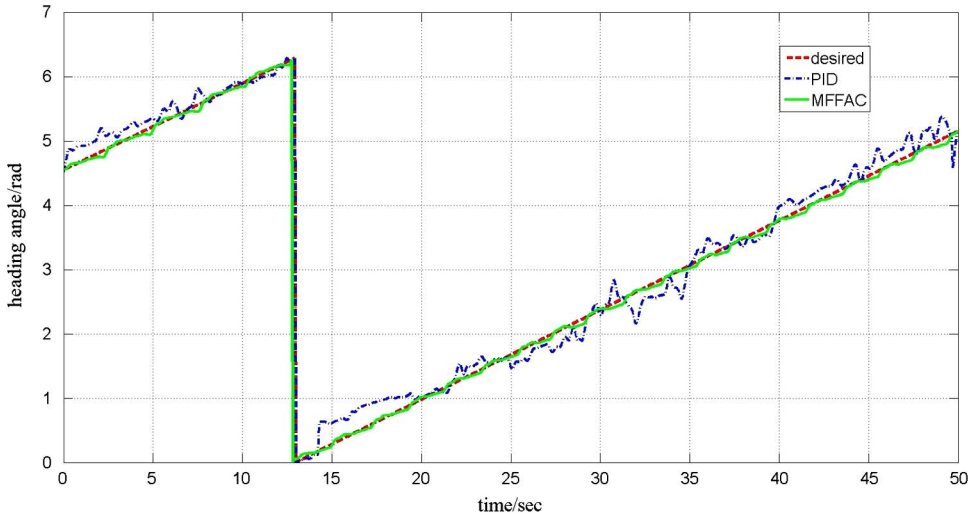

Fig. 5. Case 1: Heading angle of the UAV in the face of a fixed value of the angle rate (0.1 rad/s) and turbulence wind (5 knots)

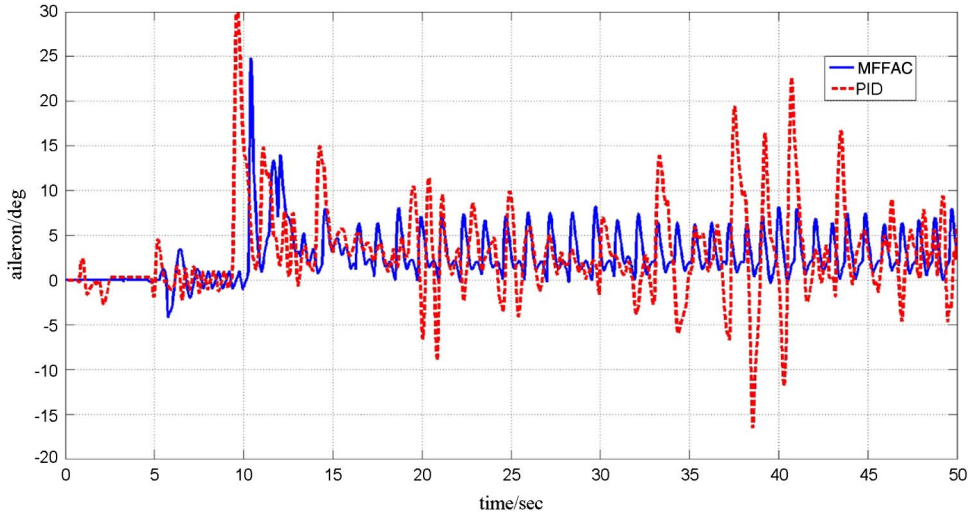

Fig. 6. Control inputs of the aileron with a turbulent wind

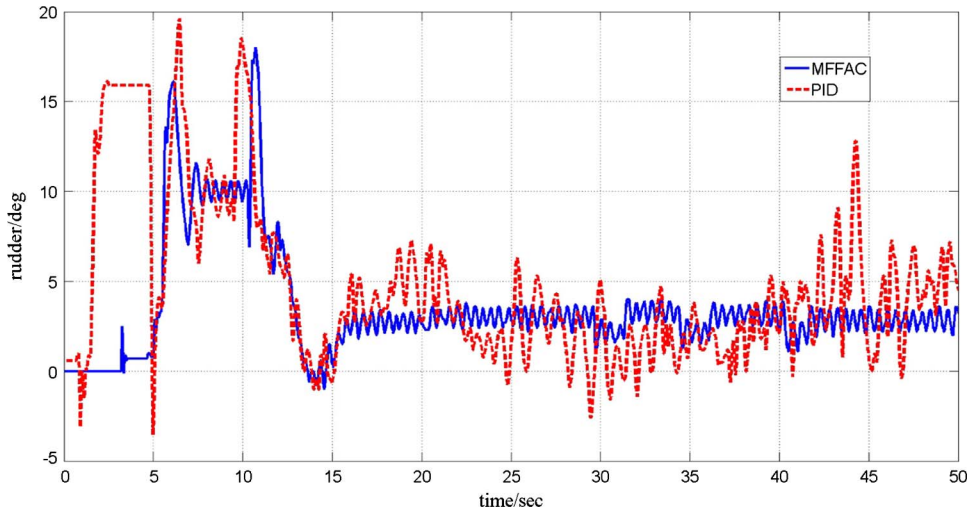

Fig. 7. Control inputs of the rudder with a turbulent wind

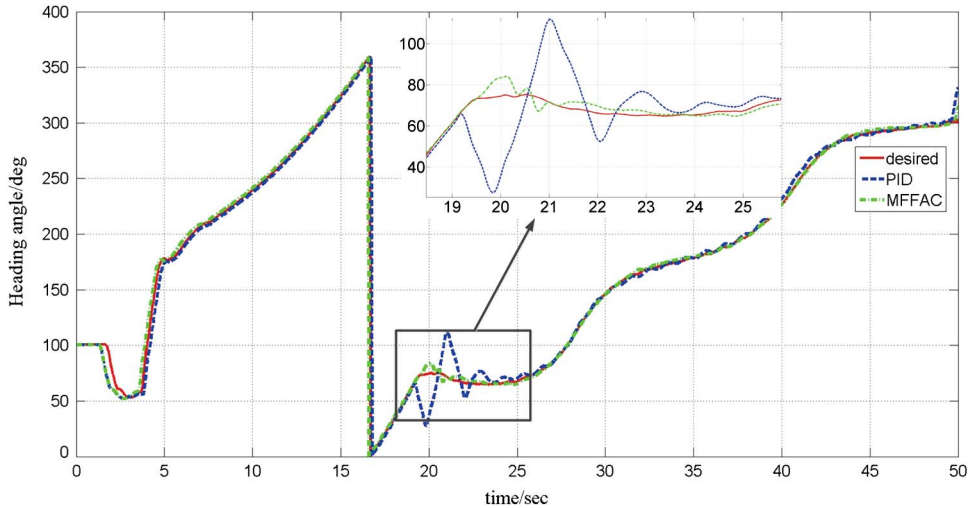

Fig. 8. Case 2: Heading angle of the UAV in the face of a changeable value of the angle rate and gust wind (10 knots)

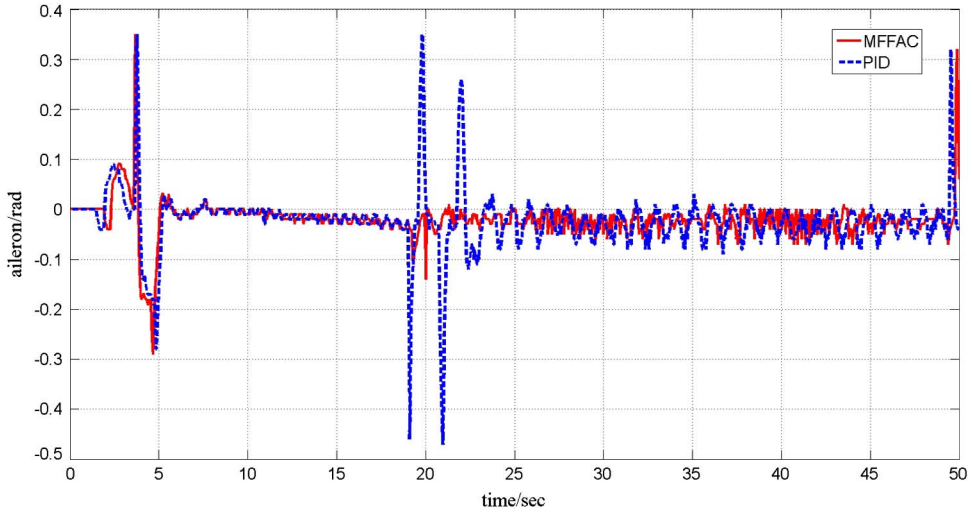

Fig. 9. Control inputs of the aileron with a gust wind

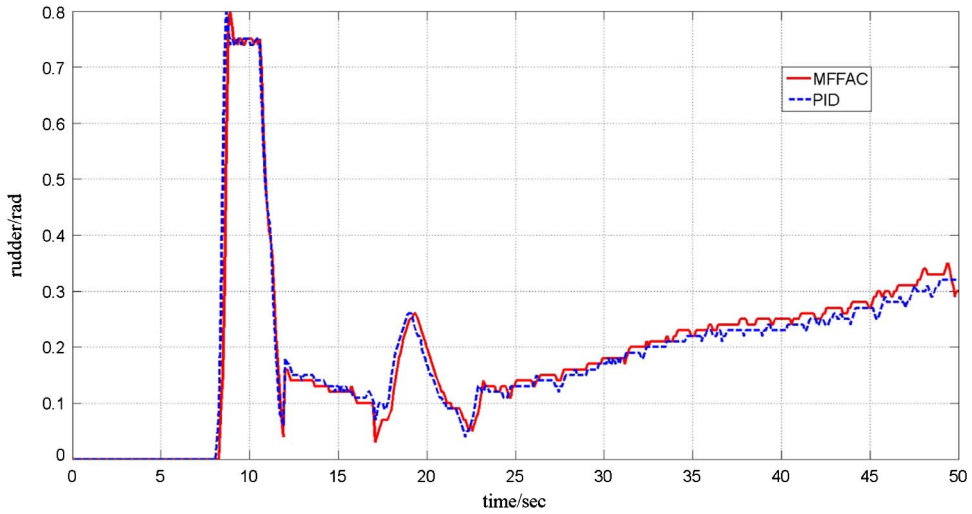

Fig. 10. Control inputs of the rudder with a gust wind

difference when the heading of the vehicle is perpendicular to the direction of the wind (18–25 s in the figure). That is because the sliding effect gradually increases, and the negative adjustments of the rudder are out of work. The overshoot of the PID controller is up to 0.8 rad, in comparison with 0.2 rad of the proposed method. The control inputs of the aileron and the rudder are presented in Figs. 9 and 10, respectively.

Conclusion

In this paper, the authors have proposed a model-free fuzzy adaptive control strategy to control the heading angle of fixed-wing UAVs. Based on the dynamic linearization technology, the nonlinear kinematic equation of the motion of the heading angle has been converted into a simple and easy form, which is estimated by I/O data in every control loop. By employing the adaptive fuzzy neural network, the PPD has been estimated and the corresponding control scheme has been designed. Accurate and stable control is achieved with the designed strategy, and high-fidelity semiphysical simulations with an X-plane illustrate the effectiveness and applicability of the proposed control strategy. The proposed algorithm is not only easy to implement, but also significantly improves the system performance even if the random disturbances are not negligible.

Future work will focus on the altitude control problem of UAVs subject to disturbances and will be extended to other dimensional motions. In addition, the control input constraints and the minimum turn radius of the UAV also need to be considered.

Appendix I. Proof of Lemma 2

Proof: Determine the derivative of $J_\Phi(k)$ with respect to $\theta(k)$

$$\begin{aligned}\frac{\partial J_\Phi(k)}{\partial \theta(k)} &= \frac{\partial J_\Phi(k)}{\partial \Phi(k)}\frac{\partial \Phi(k)}{\partial \theta(k)} \\ &= \{[\pi + \Delta u^2(k-1)]\hat{\Phi}(k) - \pi\hat{\Phi}(k-1) \\ &\quad - \zeta \Delta y(k)\Delta u(k-1)\}\xi(k) \end{aligned} \tag{41}$$

Substituting (41) into (23),

$$\begin{aligned}\theta(k+1) &= \theta(k) - \gamma(k)\frac{\partial J_\Phi(k)}{\partial\theta(k)} = \theta(k)\\ &\quad - \gamma(k)\{[\pi + \Delta u^2(k-1)]\hat{\Phi}(k)\\ &\quad - \pi\hat{\Phi}(k-1) - \cdots - \zeta\Delta y(k)\Delta u(k-1)\}\xi(k)\\ &= \theta(k) - \gamma(k)[\pi + \Delta u^2(k-1)]\theta(k)\xi^2(k)\\ &\quad - [\pi\hat{\Phi}(k-1) - \cdots - \zeta\Delta y(k)\Delta u(k-1)]\xi(k)\\ &= \theta(k)\{1 - \gamma(k)[\pi + \Delta u^2(k-1)]\xi^2(k)]\\ &\quad - [\pi\hat{\Phi}(k-1) - \cdots - \zeta\Delta y(k)\Delta u(k-1)\}\xi(k)\\ &= \theta(k)\Lambda_1(k) - \Lambda_2(k) \end{aligned} \tag{42}$$

where $\Lambda_1 = 1 - \gamma(k)[\pi + \Delta u^2(k-1)]\xi^2(k)$ and $\Lambda_2 = [\pi\hat{\Phi}(k-1) - \zeta\Delta y(k)\Delta u(k-1)]\xi(k)$.

According to the definition of $\xi(k)$, it is clear that $|\xi(k)| < 1$. Then, one can obtain

$$|\Lambda_1| < 1, \qquad \Lambda_2 < 0 \tag{43}$$

so $\theta(k)$ is bounded. From $\hat{\Phi}(k) = \theta^T(k)\xi(k)$, one can see that $\hat{\Phi}(k)$ is bounded as well.

Acknowledgments

This work is supported by the National Natural Science Foundation (NNSF) of China under Grant 61403406.

References

Beard, R. W., Ferrin, J., and Humpherys, J. (2014). "Fixed wing UAV path following in wind with input constraints." *IEEE Trans. Control Syst. Technol.*, 22(6), 2103–2117.

Beard, R. W., McLain, T. W., Goodrich, M. A., and Anderson, E. P. (2002). "Coordinated target assignment and intercept for unmanned air vehicles." *IEEE Trans. Rob. Autom.*, 18(6), 911–922.

Brezoescu, A., Espinoza, T., Castillo, P., and Lozano, R. (2013). "Adaptive trajectory following for a fixed-wing uav in presence of crosswind." *J. Intell. Rob. Syst.*, 69(1), 257–271.

Cabecinhas, D., Silvestre, C., Rosa, P., and Cunha, R. (2007). "Path-following control for coordinated turn aircraft maneuvers." *AIAA Guidance, Navigation and Control Conf. and Exhibit*, AIAA, Hilton Head, SC.

Cai, G., Chen, B. M., Peng, K., Dong, M., and Lee, T. H. (2008). "Modeling and control of the yaw channel of a UAV helicopter." *IEEE Trans. Ind. Electron.*, 55(9), 3426–3434.

Chao, H., Cao, Y., and Chen, Y. (2007). "Autopilots for small fixed-wing unmanned air vehicles: A survey." *2007 Int. Conf. on Mechatronics and Automation*, IEEE, Piscataway, NJ, 3144–3149.

Chao, H., Cao, Y., and Chen, Y. (2010). "Autopilots for small unmanned aerial vehicles: a survey." *Int. J. Control Autom. Syst.*, 8(1), 36–44.

Guo, Y., and Liu, J. (2012). "Neural network based adaptive dynamic surface control for flight path angle." *2012 IEEE 51st IEEE Conf. on Decision and Control (CDC)*, IEEE, Piscataway, NJ, 5374–5379.

Hou, Z., and Bu, X. (2011). "Model-free adaptive control with data dropouts." *Expert Syst. Appl.*, 38(8), 10709–10717.

Hou, Z., and Jin, S. (2011a). "A novel data-driven control approach for a class of discrete-time nonlinear systems." *IEEE Trans. Control Syst. Technol.*, 19(6), 1549–1558.

Hou, Z., and Jin, S. (2011b). "Data-driven model-free adaptive control for a class of MIMO nonlinear discrete-time systems." *IEEE Trans. Neural Networks*, 22(12), 2173–2188.

Hou, Z.-S., and Wang, Z. (2013). "From model-based control to data-driven control: Survey, classification and perspective." *Inf. Sci.*, 235, 3–35.

Jang, J.-S., and Sun, C.-T. (1995). "Neuro-fuzzy modeling and control." *Proc., IEEE*, 83(3), 378–406.

Luo, Y., Chao, H., Di, L., and Chen, Y. (2011). "Lateral directional fractional order (pi) control of a small fixed-wing unmanned aerial vehicles: Controller designs and flight tests." *IET Control Theory Appl.*, 5(18), 2156–2167.

Mahony, R., Beard, R. W., and Kumar, V. (2016). "Modeling and control of aerial robots." *Springer handbook of robotics*, Springer, New York, 1307–1334.

Mystkowski, A. (2013). "Robust control of the micro UAV dynamics with an autopilot." *J. Theor. Appl. Mech.*, 51(3), 751–761.

Nabaa, N., and Bishop, R. H. (2000). "Validation and comparison of coordinated turn aircraft maneuver models." *IEEE Trans. Aerosp. Electron. Syst.*, 36(1), 250–259.

Paw, Y. C., and Balas, G. J. (2011). "Development and application of an integrated framework for small UAV flight control development." *Mechatronics*, 21(5), 789–802.

Poksawat, P., Wang, L., and Mohamed, A. (2016). "Automatic tuning of attitude control system for fixed-wing unmanned aerial vehicles." *IET Control Theory Appl.*, 10(17), 2233–2242.

Ren, W., and Beard, R. W. (2004). "Trajectory tracking for unmanned air vehicles with velocity and heading rate constraints." *IEEE Trans. Control Syst. Technol.*, 12(5), 706–716.

Sujit, P., Saripalli, S., and Sousa, J. B. (2014). "Unmanned aerial vehicle path following: A survey and analysis of algorithms for fixed-wing unmanned aerial vehicles." *IEEE Control Syst.*, 34(1), 42–59.

Wang, N., and Er, M. J. (2016). "Direct adaptive fuzzy tracking control of marine vehicles with fully unknown parametric dynamics and uncertainties." *IEEE Trans. Control Syst. Technol.*, 24(5), 1845–1852.

Wang, N., Er, M. J., Sun, J.-C., and Liu, Y.-C. (2016a). "Adaptive robust online constructive fuzzy control of a complex surface vehicle system." *IEEE Trans. Cybern.*, 46(7), 1511–1523.

Wang, N., Sun, J.-C., Er, M. J., and Liu, Y.-C. (2016b). "A novel extreme learning control framework of unmanned surface vehicles." *IEEE Trans. Cybern.*, 46(5), 1106–1117.

Warsi, F. A., et al. (2014). "Yaw, pitch and roll controller design for fixed-wing UAV under uncertainty and perturbed condition." *Signal Processing and Its Applications (CSPA), 2014 IEEE 10th Int. Colloquium*, IEEE, Piscataway, NJ, 151–156.